TREE RING EVIDENCE OF A 22-YEAR RHYTHM OF DROUGHT AREA IN WESTERN UNITED STATES AND ITS RELATIONSHIP TO THE HALE SOLAR CYCLE

Charles W. Stockton

and

David M. Meko

The Laboratory of Tree-Ring Research

The University of Arizona

Tucson, Arizona 85721

J. Murray Mitchell, Jr.

National Oceanic and Atmospheric Administration

Environmental Data and Information Service

Silver Spring, MD 20910

paper to be presented at the meeting of Working Group VIII under the US/USSR Agreement of Protection of the Environment, held at the Crimean Astrophysical Observatory and the Kislovosk Mountain Observatory, Russia, on 13-23 September 1978.

Introduction

For some time now, there has been considerable conjecture that major droughts affecting the Northern Hemisphere, especially the North Amercian continent, have a tendency to occur in approximately 22-year periodicities (eg. Willett 1965, Palmer 1964, Thompson 1973, Roberts 1973). However, because of the relatively short duration of the meteorological data base, this assumed near 22-year periodicity in drought has been difficult to demonstrate. During the past three years, research at the Laboratory of Tree-Ring Research at the University of Arizona has investigated the possible use of tree-ring data series as proxy data for extending knowledge of spatial and temporal drought frequency in western North America. Initial results based on roughly 360 years of drought area indices reconstructed from tree-ring data, show a tendency for a rhythmic return period near 22 years in length, for large-scale drought occurrences.

Data

The Palmer Drought Severity Index (Palmer 1965) is used as an indicator of the severity and duration of drought periods. This PDSI index, developed by W.C. Palmer of the U.S. Weather Bureau, is based on an empirical water balance approach. The Thornthwaite method (Thornthwaite 1948, Thornthwaite and Mather 1955) of computing Potential Evapotranspiration from readily available precipitation and temperature data forms a basis for calculating the climatic demand for moisture and the subsequent development of the PDSI. The PDSI for a given month is determined partly by the value of the Index for the preceding month through an autoregressive relationship and partly from moisture received during the month in question. A moisture anomaly is defined as the departure of the actual precipitation received from that expected under "normal" moisture conditions. The "expected" precipition is calculated by the water balance approach and takes into account accumulated soil moisture levels and estimated evapotranspiration.

The PDSI scale is shown on Table 1. The PDSI, for which maps are published monthly by the National Oceanic and Atmospheric Administration in the Weekly Weather and Crop Bulletin, has the desirable property that a given PDSI value means roughly the same degree of drought from one location to another. Also, the PDSI is an integrative index of moisture conditions similar to the response recorded in tree-ring width series. From a hydrologic standpoint, the PDSI is a desirable index for slower response systems such as fluctuations in groundwater levels and in storage in large reservoirs.

The data used in this portion of the study were obtained from the National Climatic Data Center in Asheville, North Carolina, and consisted of monthly PDSI values for each of the climatic divisions in the United States for the period 1931-1970. The area studied was restricted to roughly the

TABLE 1

DROUGHT CLASSIFICATION BY PALMER
DROUGHT SEVERITY INDEX (PDSI)

Palmer index	Degree of drought
PDSI $\leq$ -4.0	Extremely dry
-4.0 $<$ " $\leq$ -3.0	Severely dry
-3.0 $<$ " $\leq$ -2.0	Moderately dry
-2.0 $<$ " $\leq$ -1.0	Mildly dry
-1.0 $<$ " $<$ +1.0	Near normal
+1.0 $\leq$ " $<$ +2.0	Mildly wet
+2.0 $\leq$ " $<$ +3.0	Moderately wet
+3.0 $\leq$ " $<$ +4.0	Severely wet
+4.0 $\leq$ "	Extremely wet

states west of the Mississippi River, comprising 204 climatic divisions. Since our interest lay mainly with large-scale drought patterns, the 204 divisions were grouped into 40 regions (Figure 1a), using the rainfall classification scheme of Trewartha (1961). Regional PDSI series were then calculated as the arithmetic mean of the PDSI of the divisions within each group.

Since drought was to be reconstructed from annual tree-ring indices, while the regional PDSI series consisted of monthly values, it was necessary to derive from the PDSI series some annual measure of drought that would be expected to yield a strong relationship to tree growth. The July PDSI was chosen for the following reasons: annual tree growth as reflected in the ring widths is usually nearly complete by the end of July; July PDSI reflects to some degree the moisture conditions of the prior spring and late winter -- these conditions are relatively important to most of the species of trees used in this study; major droughts from 1931-1970 tended to peak in intensity during July or August; and July PDSI is particularly important in the growth and yield of agricultural crops.

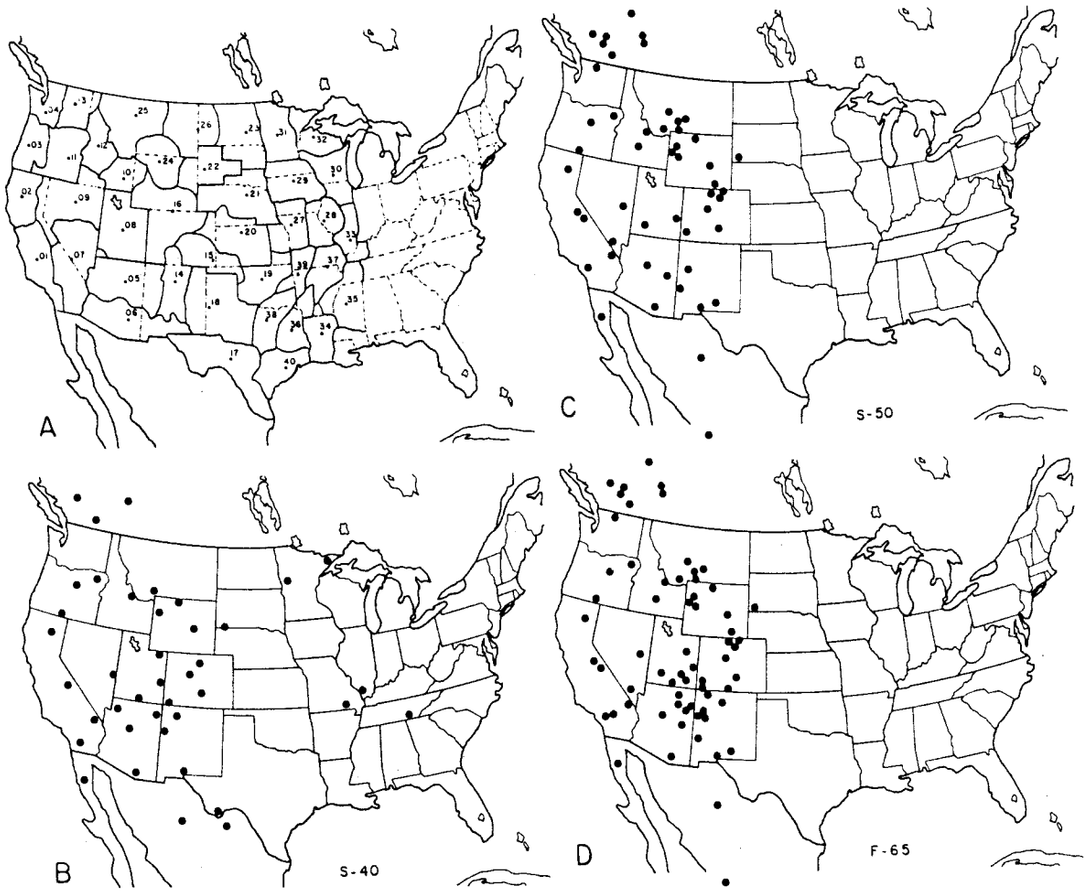

Figure 1. Domain of drought analysis on which this study is based. 1(A): Areas with solid boundaries and interior numbers identify the 40 climatic regions in which Palmer Drought Severity Index was observed or reconstructed. 1(B): Spatial distribution of tree-ring data sites designated as S-40, used in reconstructing PDSI to 1700 A.D. 1(C): Spatial distribution of tree-ring sites designated as S-50, used in reconstructing PDSI to 1601 A.D. 1(D): Spatial distribution of tree-ring sites designated as F-65, used in reconstructing PDSI to 1600 A.D.

The tree-ring data grids used in the analysis consisted of 40, 50 and 65 (Fritts and Shatz 1975) tree-ring sites chosen on the basis of replication, location and sensitivity to climatic variation. In general, a site consists of 10 trees with 2 samples taken from each tree (Fritts 1976). Each sample, after collection was surfaced, dated, and measured as described by Stokes and Smiley (1968). Species include Pinus spp., Psuedotusga Menziessi and some Quercus spp. (S-40 Grid). Grid S-40 (Figure 1b) covers the period 1700-1962 and Grids S-50 and F-65 (Figures 1c and 1d) cover the time period 1600-1962. These data were not collected specifically for this analysis but existed in the files at the Laboratory of Tree-Ring Research. Unfortunately, there are few sites available in the relatively treeless sections of the central Great Plains; however sites do exist around the north, south and eastern portions (Grid S-40) and these have been utilized along with the more adequate coverage of sites in the western portion. Since the beginning of the study, additional sites have been collected in the southern Great Plains and these data are presently being incorporated into an enlarged grid from which additional large-scale drought reconstructions are to follow. Grids S-50 and F-65 do not possess the spatial coverage of Grid S-40 but were chosen to extend the time span of the drought reconstructions back to 1600, a period encompassing the Maunder Minimum (Eddy 1976). Thus, of the three tree-ring data grids used, the first maximizes spatial coverage and the second and third temporal coverage using existing tree-ring data.

Technique of Reconstruction

An empirical orthogonal function analysis was performed on both the PDSI and tree-ring data grids to define a smaller number of variables accounting for

most of the spatial and temporal variability in both series (Fritts 1976). Empirical orthogonal function analysis enables fields of highly correlated data to be represented adequately by a smaller number of orthogonal functions (eigenvectors) and corresponding orthogonal amplitudes. Kutzbach (1967) provides a detailed explanation of the mathematical procedure necessary to define the functions and their amplitudes.

Empirical orthogonal functions (eigenvectors) of the PDSI were computed from the 40 observations of July PDSI (1931-1970) in the 40 regions (Figure 1a). The analysis indicated the 40 original spatial patterns of PDSI could be represented quite well by the first five eigenvectors explaining (75%) of the variance. The first eigenvector accounts for 38 percent, the second 17, and the third 11 percent. The remaining fourth and fifth account for about 10 percent.

A similar analysis was performed on the 264-year record (1700-1963) of tree-ring indices for the 40 sites of Grid S-40 and for the 364-year record (1600-1963) for Grids S-50 and F-65. The first 10 eigenvectors accounted for about 60 percent of the variation with the first five of these representing nearly 50 percent of the total variance. The tree-ring record overlapped the PDSI record for the years 1931-1963, and these years were used to derive a transfer function for reconstruction (See Appendix I). The approach to reconstructing the long term drought record consisted of deriving relationships to predict PDSI amplitudes from tree-ring amplitudes using canonical analysis (Fritts, Blasing, Hayden, Kutzbach 1971). For Grid S-40 a total of 6 amplitudes were used, accounting for 45 percent of the total variance; in the S-50 grid case, only the first two amplitudes were used, but they were entered into the transfer function such that drought at time t was compared with tree-ring data

over the times t + 1, and t - 1, for a total of 6 variables. The first two amplitudes account for 32% of the total variance in the 50 station tree-ring data grid over the time 1931-1962. The information for all grids is summarized in Table 2.

Canonical analysis was used to derive a matrix of least squares coefficients to predict amplitudes derived from the first five PDSI eigenvectors from the amplitudes of tree-ring series eigenvectors. The resulting transfer

TABLE 2

DROUGHT AREA RECONSTRUCTIONS

GRID	(A) TREE-RING INDICES				(B) DROUGHT INDICES (PDSI)			
	Period of Record	Data Points	EVs# Retained	Variance Explained	Period of Record	Data Points	EVs# Retained	Variance Explained
S-40	1700-1962	40	6	45%	1931-1970	40	5	75%
S-50	1600-1962	50	2	31%	1931-1970	40	7	83%
F-65	1600-1962	65	3	41%	1931-1970	40	5	75%

DAI FAMILY	(C) CANONICAL "BRIDGE"[1]		(D) DAI VARIANCE EXPLAINED*			
			PDSI LIMIT			
	Terms Retained	Variance In Common*	<-1	<-2	<-3	<-4
S-40	5	64%	72%	72%	74%	78%
S-50	6	56%	67%	76%	79%	75%
F-65	5	65%	69%	70%	79%	74%

*In overlap period 1931-1962 (32 years)
#EVs = Eigenvectors

PDSI = Palmer Drought Severity
DAI = Drought Area Index

1. The maximum number of "terms retained" can not exceed the smallest number of variables in either set. The variables for the tree-ring set included the amplitudes lagged so that the PDSI amplitudes at time t are compared with those from the tree-ring set at times t and t + 1 (Grids S-40, and F-65) and t , t + 1, and t - 1, (Grid S-50). See Stockton (1965) for justification of the lagged variables.

function explained about 64 percent of the variance of the PDSI amplitude series during the calibration period (1931-1963) for Grid S-40 and about 56 percent for Grid S-50 and 65 percent for Grid F-65.

This same transfer function was then applied to the 1700-1962 and 1600-1963 tree-ring amplitude series and in this manner the amplitudes of the PDSI were reconstructed back to 1700 (Grid S-40) and 1600 (Grid S-50 and F-65). Reconstructed values of the PDSI series were then obtained by multiplying the matrix of predicted PDSI amplitudes by the matrix of appropriate PDSI eigenvectors.

Details of the technique employed here are described in Appendix I.

Reconstructed Drought Index Series

Good agreement of the reconstructed values with the actual values in the period of calibration is a necessary, although not a totally sufficient condition for valid reconstruction of past conditions. It follows then, that the first step was to check the accuracy of our reconstructions during the 1931-1962 calibration period. To accomplish this, the number of regions in each of nine PDSI categories for each July from 1931-1962 was tabulated and plotted for both the 40 station grid reconstructed and actual data series. The comparison is shown in Figure 2, for the regions wetter than normal ($PDSI \geq + 1.0$) and the number of divisions drier than normal ($PDSI \leq - 1.0$). The agreement is good with the longer term variation being well duplicated. Since only the first five PDSI eigenvectors were used in the reconstruction, those years when less significant eigenvectors dominated were poorly duplicated. Such was the case in 1952 and 1962.

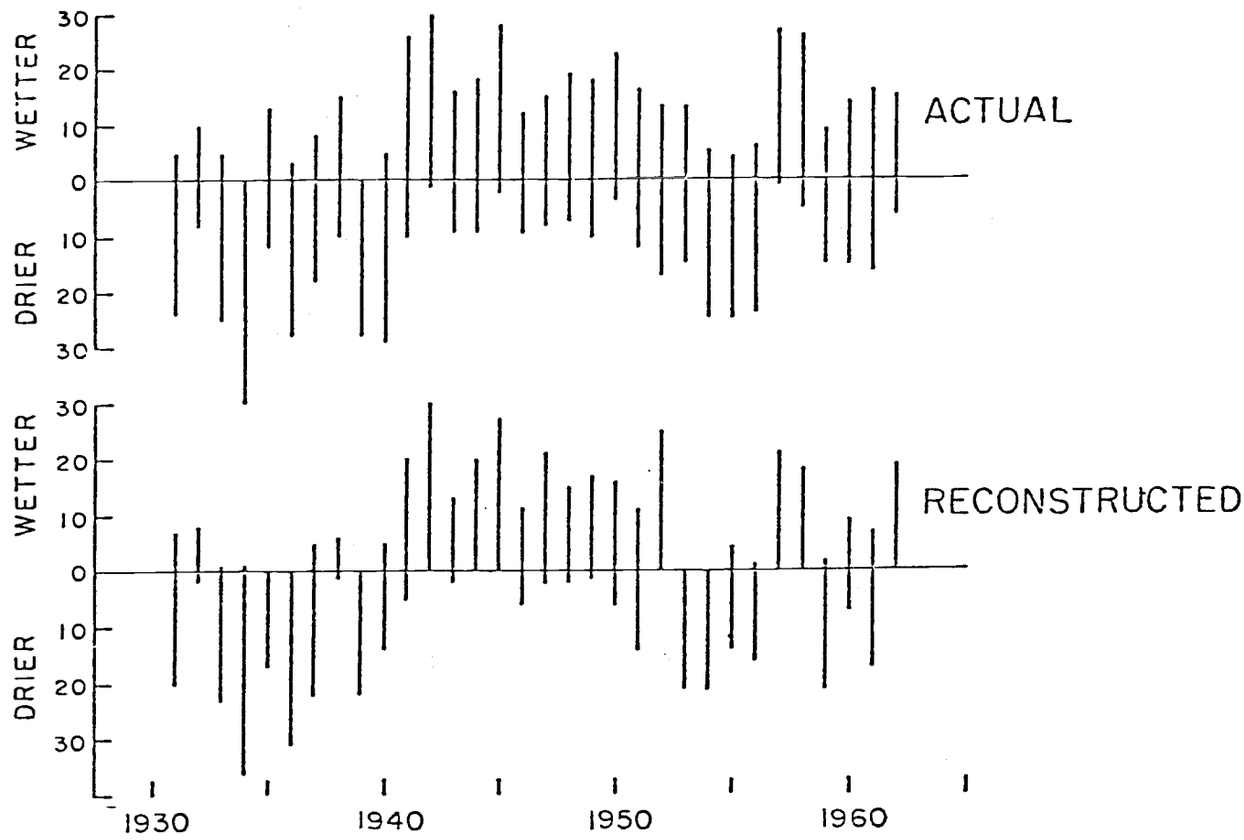

Figure 2. Number of regions drier than normal, number of regions wetter than normal; reconstructed and actual for the calibration period. Normal = (-1.0 PDSI +1.0).

As an additional measure of the accuracy of reconstructions in the calibration period we calculated the correlation coefficients between reconstructed drought areas (in terms of number of regions in a given severity of drought) and the actual drought area. Correlation coefficients were calculated between the actual series and each of 12 reconstructed series (PDSI $\leq$ -1, PDSI $\leq$ -2, PDSI $\leq$ -3, PDSI $\leq$ -4 reconstructed from each of our three tree-ring grids). The squares of the resulting correlation coefficients (Table 2d)

are estimates of the percent variance of the drought areas accounted for by the reconstructions. All percent variances are reasonably large, and results are similar for reconstructions based on different tree-ring grids.

A time series for the period 1700-1962 showing the number of regions with PDSI $\geq$ + 1.0 as opposed to those with PDSI $\leq$ - 1.0 is shown in Figure 3. Several points are apparent. First, note the rhythmic nature of the extreme wet and dry periods. It is this apparent periodic tendency that is of interest here. Moreover, it is also interesting to note that the wettest period prior to 1931 was 1914, 1915, 1916 and the driest was 1846, 1847, 1848. The driest single year in our reconstruction was 1934, the second driest, 1757. In 1934, 19 regions were in extreme drought (PDSI $\leq$ - 4.0) as compared to 10 regions in 1757.

Comparison of Reconstructions to Recorded History

We have attempted to confirm our reconstruction by two methods. First, we have compared our reconstruction with actual PDSI computed for single stations for years prior to the calibration period. Secondly, we have compared our maps of reconstructed PDSI with spatial and temporal accounts of climatic extremes taken from diary entries of travelers that crossed the Great Plains during the period 1845-1849 (Lawson and Stockton 1977). Both approaches confirm our reconstruction, but because of the technique employed to stress the large-scale features, the individual stations often provide confirmation of local rather than regional phenomena.

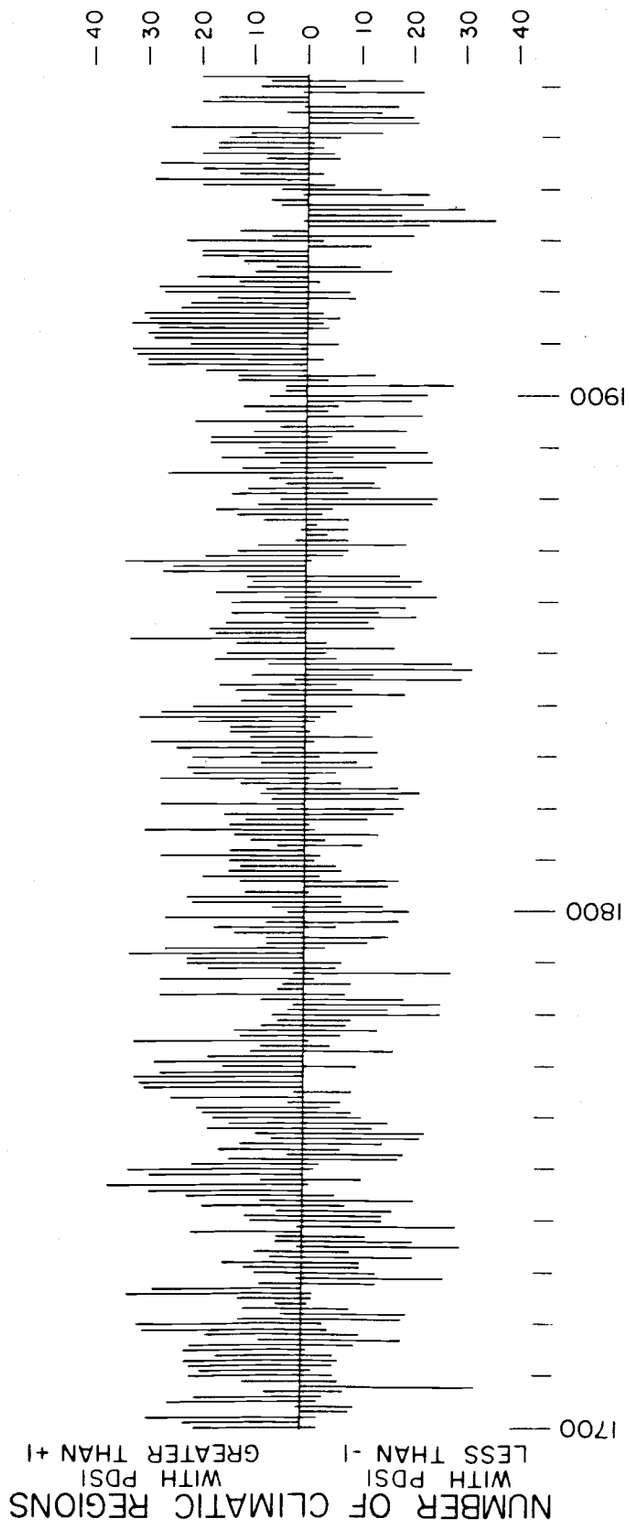

Figure 3. Number of regions reconstructed drier than normal and number of regions reconstructed wetter than normal, 1700-1962, Grid S-40.

Documentation of the Periodicity

Many past studies have been directed towards the search for periodicities in tree-ring data (Douglass 1919,1928,1936, Sirén and Hari 1971, LaMarche and Fritts 1972 and Bitvinskas 1974). In fact the origin of dendrochronology in the United States, as we know it today, can be traced to Douglass' attempts to find evidence of solar variability in tree-ring series. The sometime existence of an approximate 22-year periodicity in tree-ring data is well documented. Douglass (1946 pp. 18) noted that a periodicity of approximately 23 years was prominent in long-lived sequoias [Sequoiadendron gigantea (Lindl.) Decne.] and notes that "Schulman has found it well marked in carefully collected specimens in the intermountain (Utah) area." Douglass also noted that the period length was not constant but varied with time. In a more recent study, LaMarche and Fritts (1972), using modern statistical techniques, found that when tree-ring data were analyzed collectively on an area basis by using empirical orthogonal functions a "pair of peaks corresponding to frequencies of 22.0 and 29.2 years" appeared in the sample autospectrum. Although these peaks were significant at the 99 percent confidence level they found no significance between the amplitude series of the first eigenvector of the growth (1700-1930) and the double sunspot series when a coherence test was used.

What then makes the results reported here different from those of the past studies? Our studies differed from the earlier studies in a number of ways. 1) We have used a larger selected tree-ring data grid of 40, 50 and 65 tree-ring series covering a larger portion of the western United States and including for the first time tree-ring sites east of the Rocky Mountain states (Grid S-40). Specifically, we include in S-40 sites of white oak (Quercus alba L.)

and red oak (Quercus rubra L.), heretofore not used in this type of analysis. 2) We are analyzing the tree-ring data series after they have been converted to a Palmer Drought Severity Index series, a process that undoubtedly acts as a filter in stressing drought recurrence. 3) We are analyzing a series of reconstructed drought indices on an area basis without respect to where the area falls within the western United States and without considering whether the area is contiguous or not. 4) We have utilized in the transfer functions of PDSI with tree-ring data only the PDSI for the month of July. This could tend to amplify the emphasis of drought in the tree-ring derived reconstructed series.

We have examined whether the near 22-year periodicity can be distinguished in a drought series reconstructed from a tree-ring grid different from our original grid. H. C. Fritts and his associates in the Climatic Section of the Laboratory of Tree-Ring Research kindly reconstructed a drought series from a seperate tree-ring grid which we call F-65 (Figure 1d). In their reconstruction they used slightly different eigenvectors than were used initially in S-40 and S-50 (Table 2).

Their reconstructed drought area series was then compared with the results of the initial study by cross power spectral analysis (Jenkins and Watts 1968). The autospectrum (Figure 4a), although showing a greater percentage of low frequency variances, shows an unmistakable periodicity of 21.3 years that is significant at the 95% level if a simple autoregressive generating mechanism is assumed. When this spectrum is compared to that of the S-40 series (Figure 4b) the resulting squared coherency spectrum shows very high overall coherence (average of about .65) and a high coherence at 21.3 years (.91).

The cospectrum showing the in-phase agreement between the reconstructed

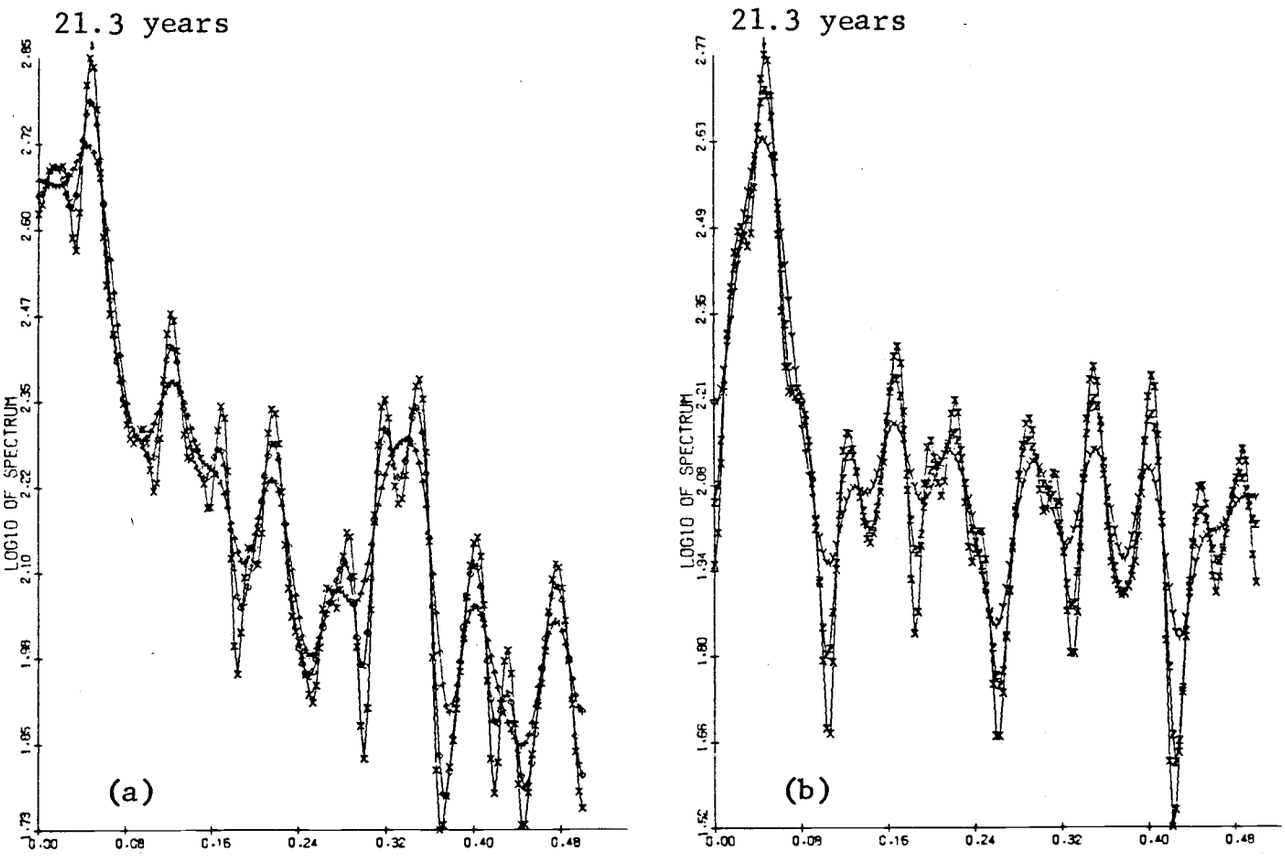

Figure 4. Autospectral functions for drought area index series as computed by Fritts group (a) and by Stockton (b). In both cases, n = 263 and d.f.= 10, 14, 21.

PDSI series also shows strong agreement at 21.3 years. This analysis clearly indicates a very strong agreement between the two reconstructed series in the 21.3 period range. In addition, it shows that our results can be independently reproduced and that the reconstructed area PDSI series derived from tree-rings show a definite periodicity of approximately 22 years. The periodicity in the initial series does not appear to be an artifact of data manipulation.

All of the prior analyses were based on the drought area index series for PDSI $\leq$ -1. It is of interest to determine if the same relationships hold

for other categories of drought. For this reason, the spectral density functions for drought area of PDSI $\leq$ -2 and for drought area PDSI $\leq$ -3 for grid S-40 were computed and compared to the function for the series PDSI $\leq$ -1 (Figure 5). It is evident that some periodic tendency diminishes in the more intense categories (e.g. PDSI $\leq$ -3).The tendency for the near 22-year periodicity is significant at the 99 percent level for the PDSI $\leq$ -1 series at the 95 percent level for the PDSI $\leq$ -2 series, but is not significant at either the 99 or 95 percent level for the PDSI $\leq$ -3 level. Comparable analyses performed on on PDSI $\leq$ -1, $\leq$ -2, $\leq$ -3 series for the other two grids show comparable results.

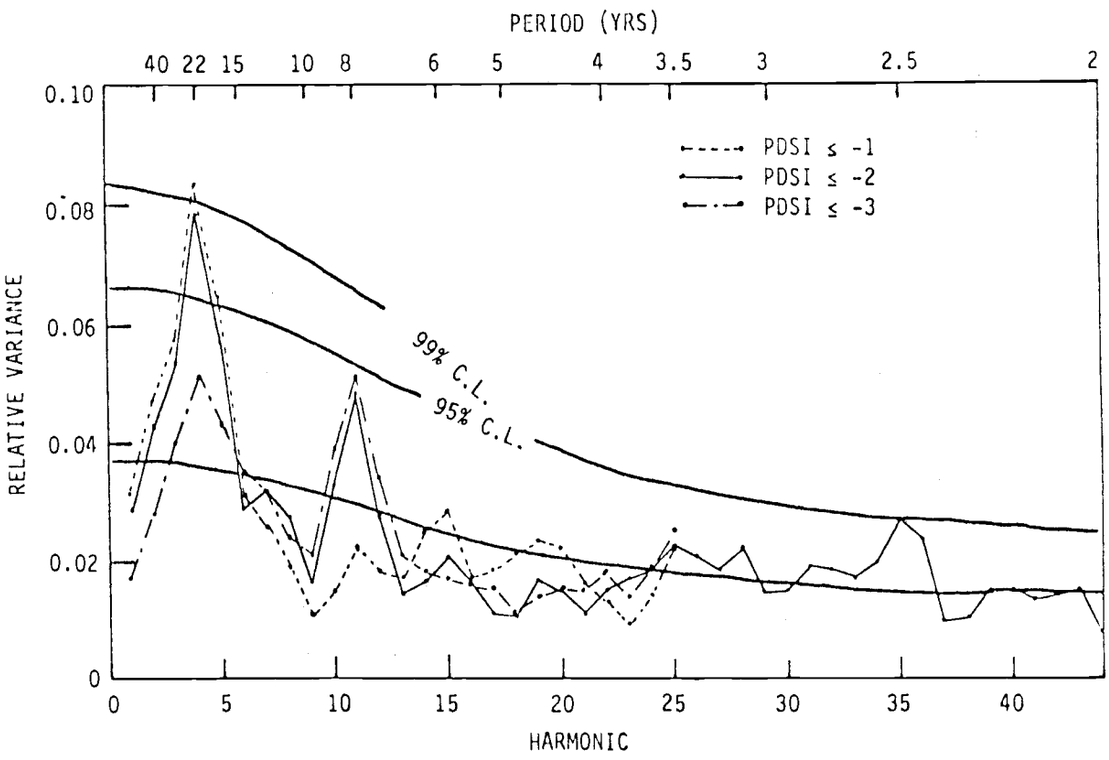

Figure 5. Spectral density functions for drought area index series, (a) PDSI $\leq$ -3, (b) PDSI $\leq$ -2, (c) PDSI $\leq$ -1. Confidence limits based on assumption of a first order Markov process generating function.

Comparison of the Area PDSI Series with the Hale Solar Cycle

It follows that the drought area index with its near 22 year periodicity should be tested for possible linkage with an appropriate geophysical series having comparable periodic characteristics. Since the Hale Double Sunspot Cycle has received considerable attention in regard to drought occurrence, various statistical tests have been performed relating the reconstructed drought area index to the double sunspot series. The consistency of the results implies a possible causal connection between drought occurrence in western United States and long-term solar variability.

Figure 6 shows the drought area index series (PDSI $\leq$ -1) from Grid S-40 after being subjected to an appropriately designed digital bandpass filter (Filter No. 1, Figure 13) that retains only the data with a return period of between 15 and 31 years. The largest weight is placed on the data with a 20.6 year return period. The double sunspot series was also subjected to the same filter. By superposing the two filtered series it is clearly evident that there is strong coherence between the periodicities of the two series, although the drought series peaks tend to lag that of the sunspot series (except during the late 1800's). It is apparent that the number of years of lag varies over the full time range of the comparison. If one assumes the nominal periodicity in the sunspot series to be 22 years and plots the drought area data as years after the alternate minimum, the results (Figure 7) show that drought tends to peak at two years following the sunspot minimum. The minimum drought area occurs at 15 years following the alternate sunspot minimum.

Two techniques have been used to evaluate this apparent phase locking between the drought area series and the double sunspot series. Harmonic dial

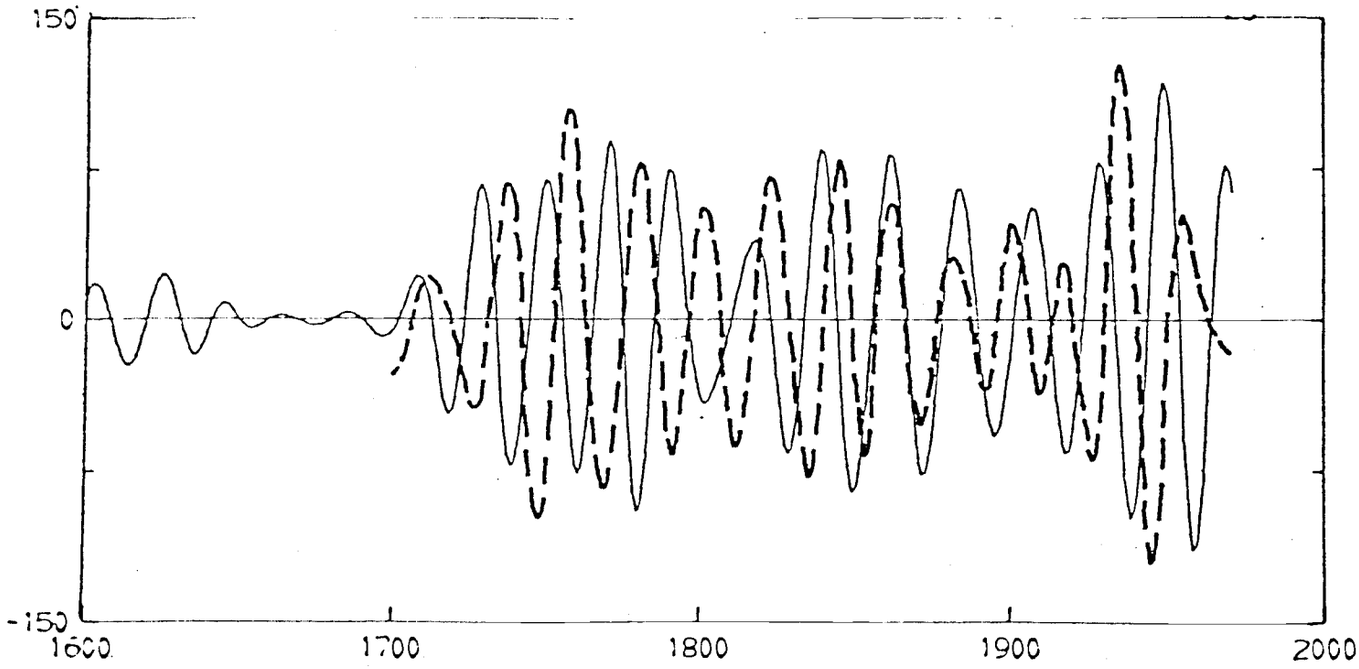

Figure 6. Plot of double sunspot series (solid line) and drought area index series (dashed line) after being filtered with a 20-year band pass filter.

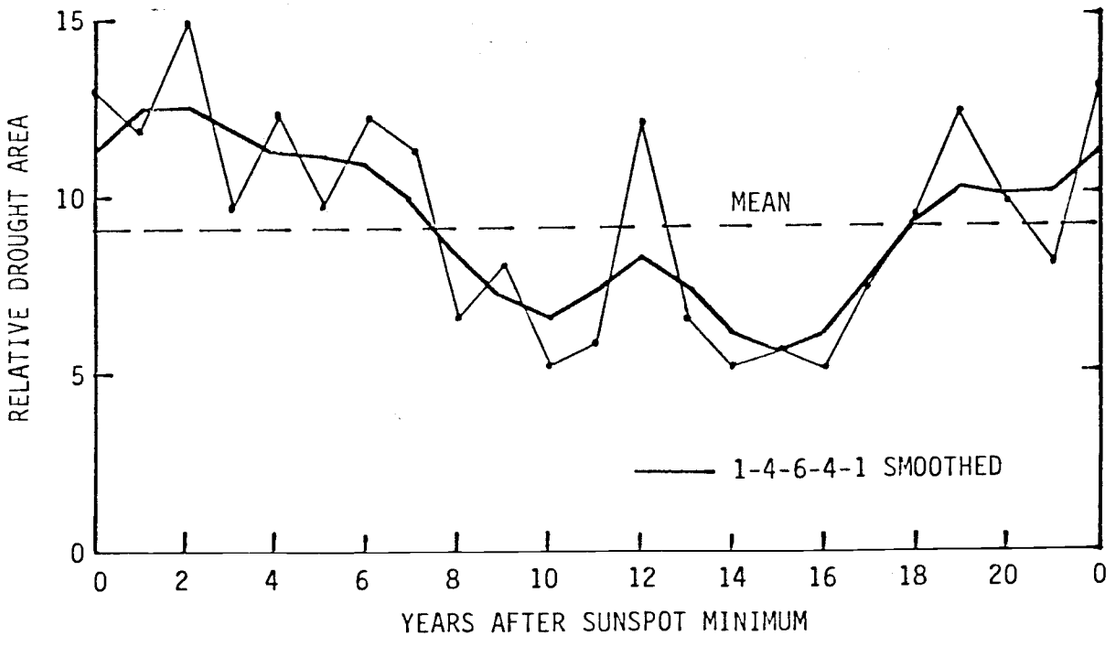

Figure 7. Relative drought area compared to years after sunspot minimum.

analysis is a convenient way of graphically depicting the phase relationship between the periodic peaks in two time series. The series are filtered by appropriately designed bandpass filters. The maxima from the filtered drought series are then plotted on the harmonic dial, where the plotted position for each drought peak depends on 1) the number of years since the preceding sunspot minimum and the number of years until the following sunspot minimum, and 2) the amplitude of the drought peak. The result (Figure 8) resembles a cluster of bullet holes in a rifle target. By computing the centroid of the cluster

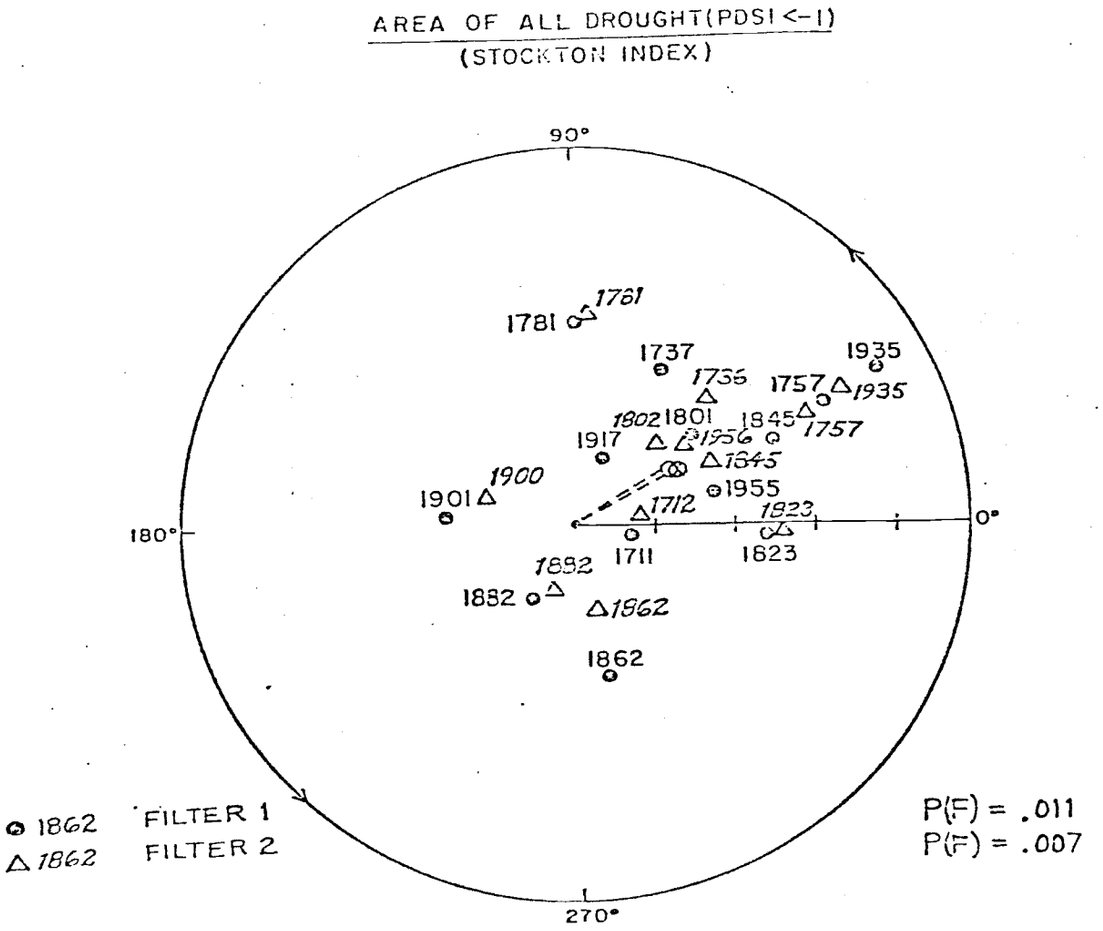

Figure 8. Harmonic dial analysis of series S-40 (PDSI $\leq$ -1), referred to Hale sunspot cycle phase. Results are shown for Filter 1 (solid circles) and for Filter 2 (open triangles). Dates of each DAI maximum are indicated. Centroids of data with Filter 1 (circle with cross) and Filter 2 (open circle) are indicated with dashed lines to origin. Beginning and ending of each Hale sunspot cycle occurs at azimuth marked 0°. Time advances counterclockwise.

and using analysis of variance, an F-test (corrected for degrees of freedom because a filtered series is used) can be used to test the significance of the phase relationship between the two series (Mitchell, Stockton, Meko, in preparation). This type of analysis has been completed for PDSI $\leq$ -1,-2,-3,-4 and all three grid reconstructions and the statistical significance appears to be better than 1% for PDSI $\leq$ -1 and -2, 2% for PDSI $\leq$ -3 and 10% for PDSI $\leq$ -4.

Cross-spectral analysis involves comparison of the two series over the entire frequency domain. The squared coherency spectrum (Figure 9) shows this comparison. As in other comparisons, we have broken the area of drought into three severity classes: all drought (PDSI $\leq$ -1), moderate and severe (PDSI $\leq$ -2),

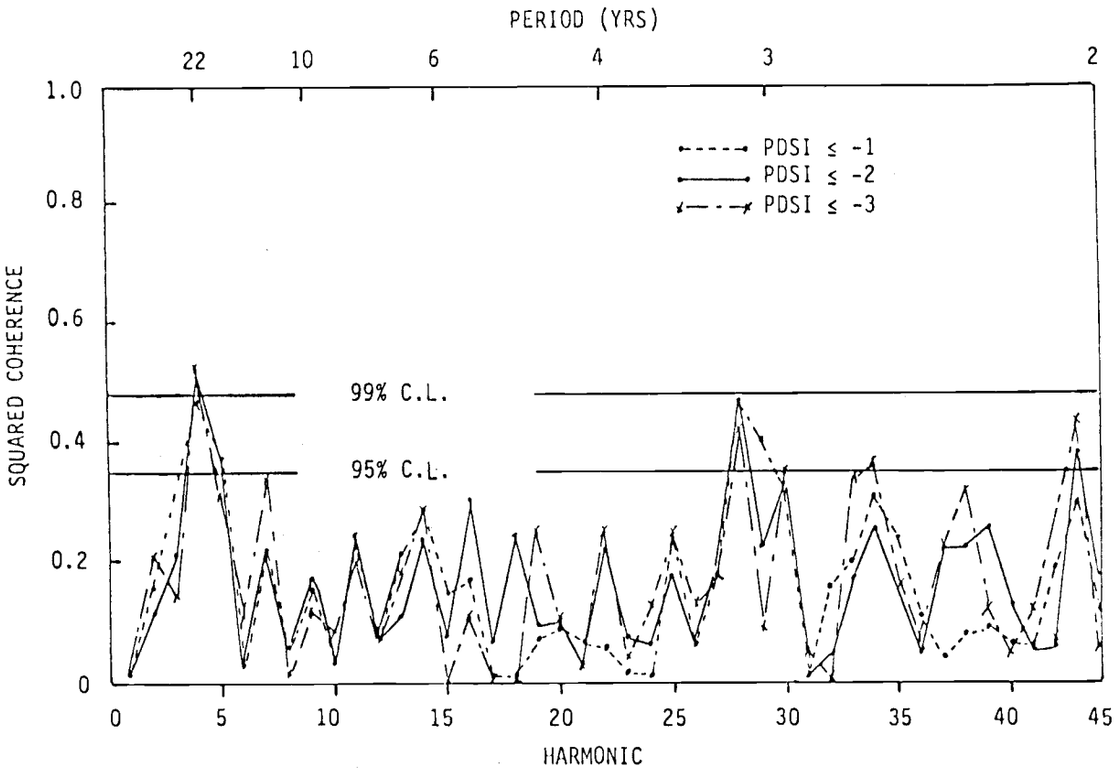

Figure 9. Coherency squared function for drought area index series versus the double sunspot series.

and severe only (PDSI $\leq$ -3). When the 95 and 99 percent confidence limits are placed on the coherency spectrum, the coherence between the drought area index series and the double sunspot series is significant (95 percent level) for all three severity classes at a period of near 22 years. At the 99 percent level only the severe category is significant at around 22 years.

Additional analysis of the time series characteristics of the drought-area series included computation of its first four moments, and the fitting of a time series generating function by the method of Box and Jenkins (1976). The Box-Jenkins analysis indicated that a first order autoregressive model provided as good a fit as any model of higher order. In fact, the persistence component is so small that the drought-area series could probably be adequately simulated with a random series having an appropriate probability distribution.

The highly skewed nature of the frequency distributions for the drought severity categories causes some concern about the placing of confidence limits on the coherency function. For this reason, we are in the process of performing a Monte Carlo simulation of the coherence.

The frequency distribution functions for each of the dry side PDSI classifications for Grid S-40 are shown on Figure 10 and it is evident that skewness increases tremendously as the drought severity index increases. We have computed the theoretical probability distribution function of best fit for each of the observed frequency distributions. The two parameter Gamma distribution provided an acceptable fit for the PDSI $\leq$ -1 series and an approximate fit for the PDSI $\leq$ -2 series although it does not pass the Chi Square test of significance at the 95% confidence level. For the other two categories, the Gumbel extreme distribution function appears to provide an acceptable fit

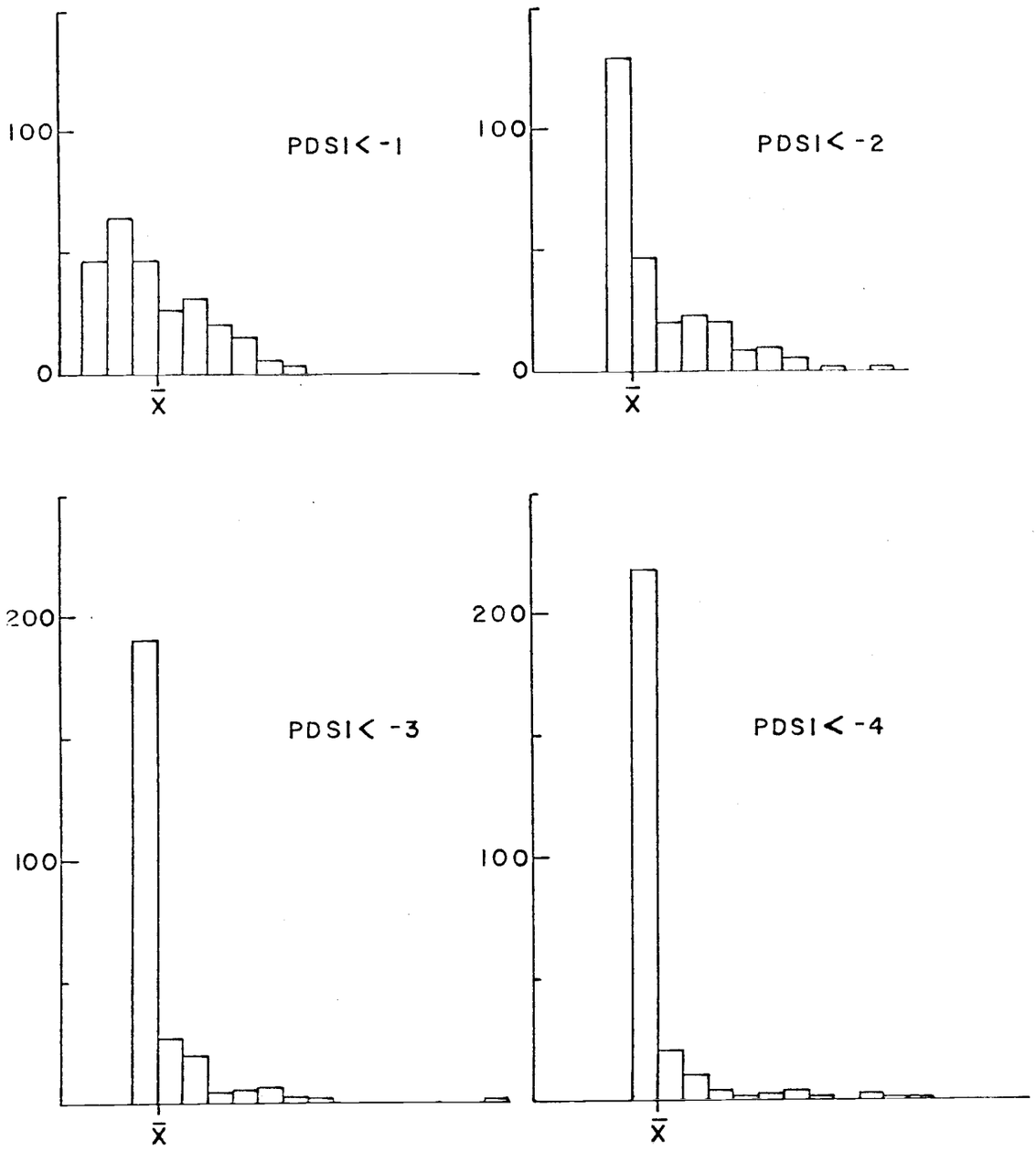

Figure 10. Number of years of occurrence of drought for July PDSI $\leq$ -1, -2, -3, -4. Total = 263. $\bar{X}$ = mean; class intervals are .5 S where S = standard deviation.

although additional work is being done on this problem.

Our objective is to create a fairly large number (e.g.1000) of simulated series 263 years long that possess the time series characteristics of the drought series including skewness and persistence but not periodicity. The coherency squared function for each of the simulated series and the double sunspot series will then be computed. Analysis of the dispersion of the computed values of the coherency will then be analyzed and the confidence limits for the coherency squared function determined.

In the original design of the investigation, Grid S-40 was carefully selected from existing tree-ring series because it maximized spatial coverage at the expense of record length. Since the original study was not intended to investigate the solar variability-drought area connection record length was not considered critical. After the discovery of the near 22-year rhythm in the drought area series, the question of the nature of our series during the Maunder Minimum period 1645-1715 became important. For that reason, the spatial constraints were relaxed in favor of those tree-ring stations providing longer data series and Grid S-50 was developed.

Reconstructed July PDSI ≤ -1 and ≤ -2 drought area series for 1601-1962 derived from Grid S-50 are shown in Figures 11 and 12. The drought area versus time plots are shown before and after being filtered with digital filters. The filters, whose response functions are shown in Figure 13, are tuned so that filter No.1 has a peak response at 20.6 years but passes the drought area data with a frequency of 15-31 years; filter No.2 has a peak response at 24.3 years but passes the original data frequencies between 18 and 36 years. The two filters were used because the original drought area series were believed to contain a rhythm with inexact wave length. In addition, we

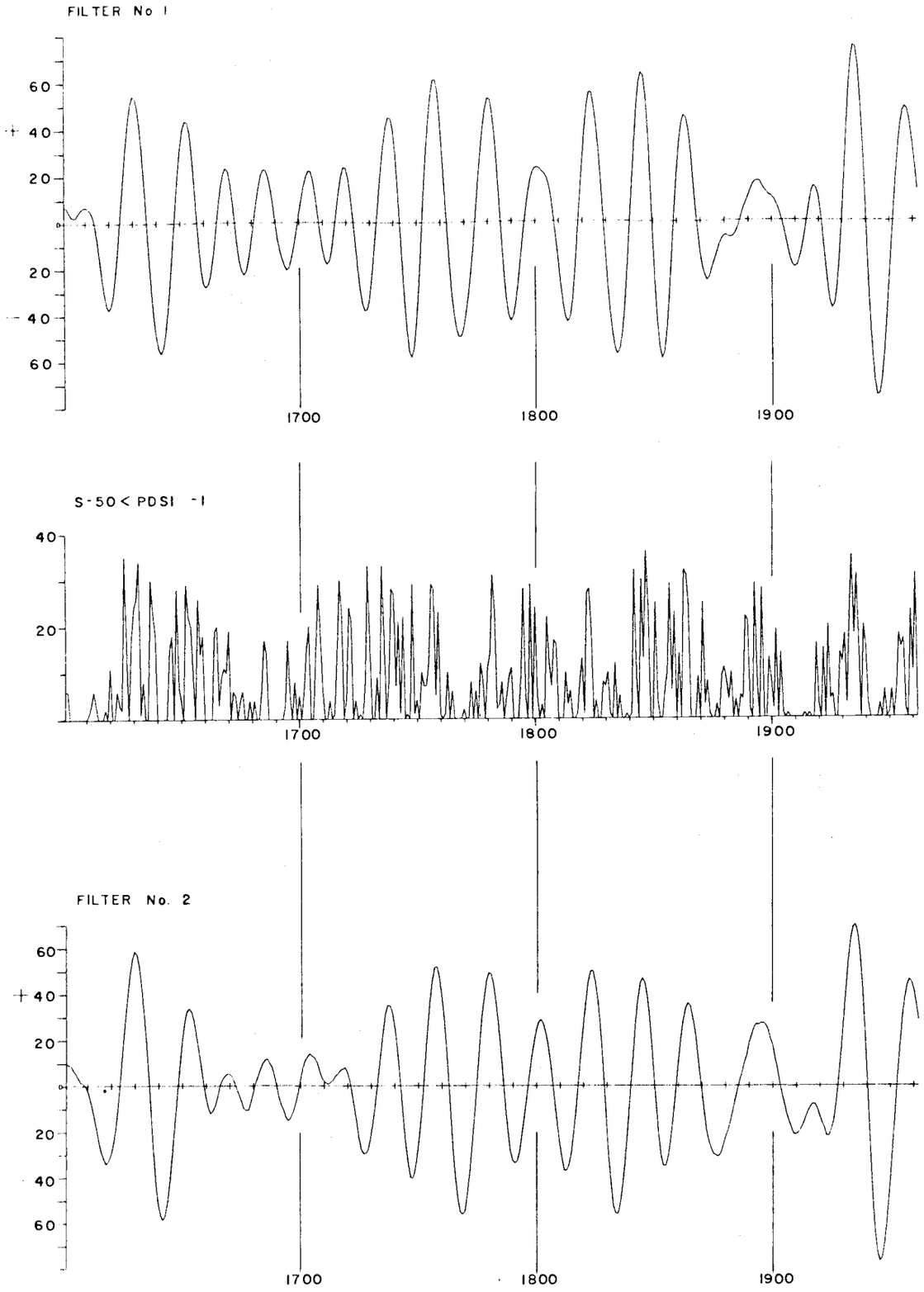

Figure 11. Drought area series for PDSI $\leq$ -1 computed from Grid S-50. Also shown are the series after being filtered with the band-pass filters (Filters No.1 and No.2) whose response functions are shown in Figure 13.

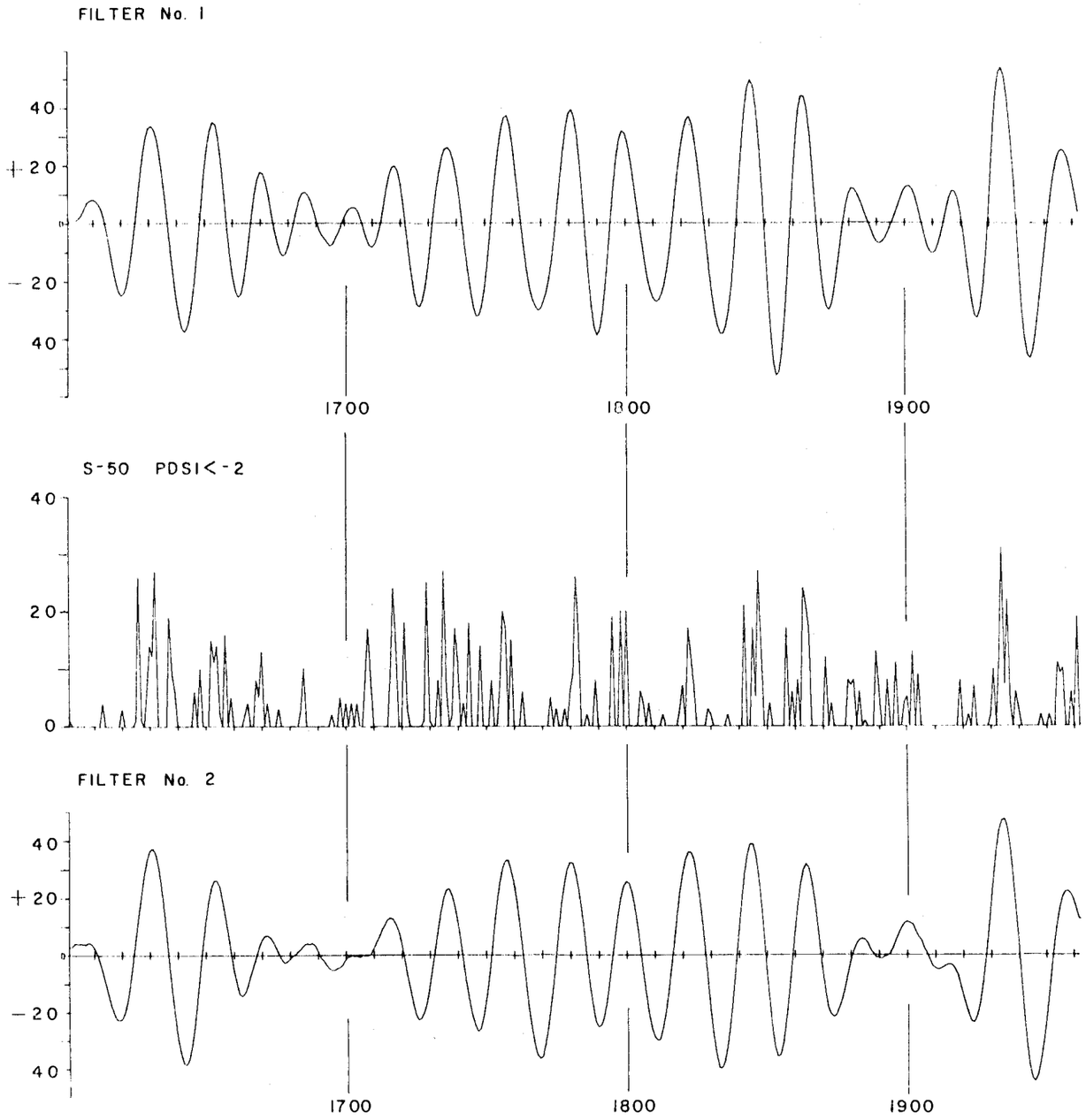

Figure 12. Drought area series for PDSI $\leq$ -2 computed from Grid shown are the series after being filtered with the band-pass filters (Filters No.1 and No.2) whose response functions are shown in Figure 13.

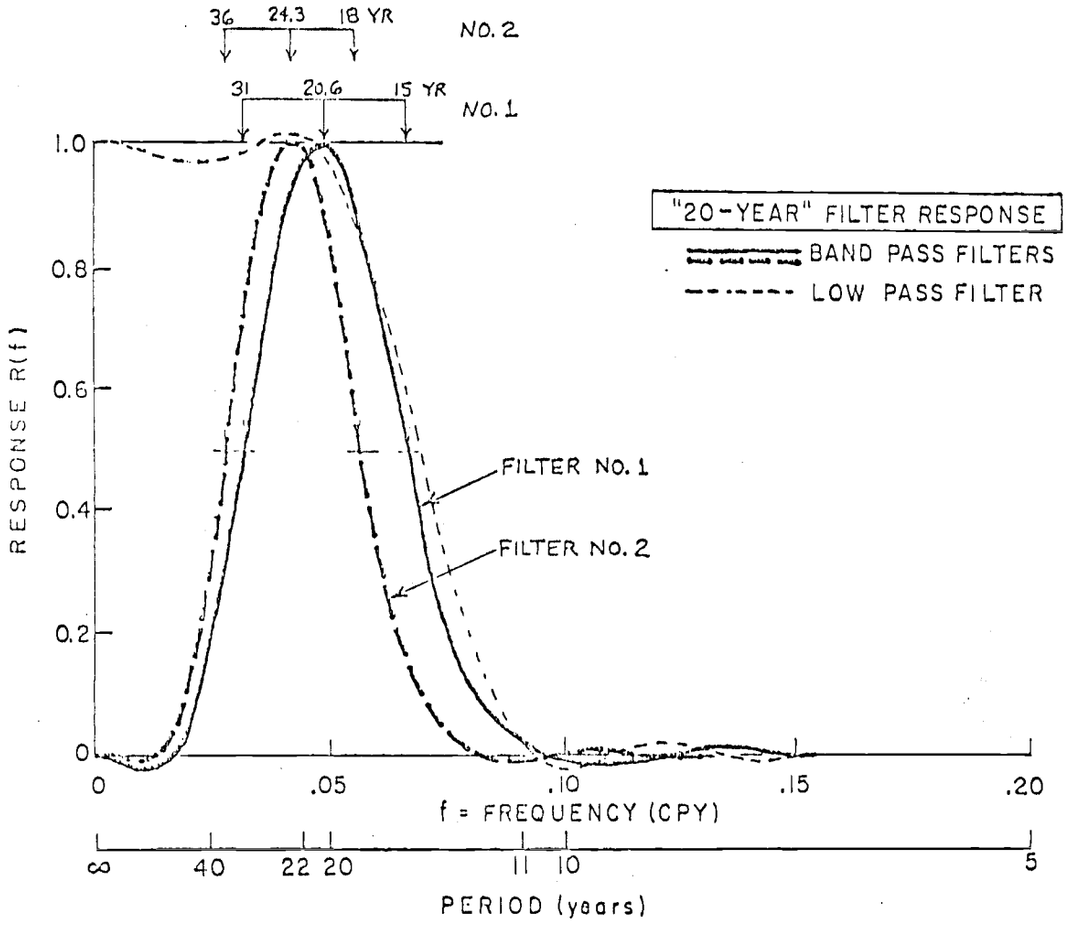

Figure 13. Response functions of band-pass filter 1 (heavy solid curve), band-pass filter 2 (heavy dashed curve). Peak response and half-response points are indicated for both band-pass filters at top (period, in years).

wanted to test the hypothesis that the original filter (No.1) was not contributing to the periodic tendencies in the data. This test involved the use of the two filtered series, harmonic dial analysis and analysis of variance. The results are detailed in Mitchell, Stockton and Meko (1979) and are not presented here. The results, however, confirm that the rhythm in the data series is not the result of filtering.

A visual comparison of the graphs of the two filtered series (Fig. 11 and 12) shows that the periodic tendencies are not grossly affected by the different filters. However, the detail of the series during the Maunder Minimum period 1645-1715 and during the early part of the 20th Century appear somewhat different. The periodic tendency seems to be better defined in the filter No.1 series, especially in the Maunder Minimum period and the early part of the 20th Century. On the contrary, results of the harmonic dial analysis (Mitchell, Stockton and Meko, 1978) indicate the phase locking between filter No.2 and the Hale sunspot series is somewhat better. Both filtered series show a well marked general lack of drought during the Maunder Minimum period. The same holds true for the period in the early 20th Century. Neither of the filtered series represent a large portion of the variance of the unfiltered series (Table 3).

We have also been studying the temporal and spatial distribution of widespread and long-lasting reconstructed droughts. Average area of drought was calculated for various 50-year and 75-year periods; the most severe periods are

		Grid		
		S-40	S-50	F-65
	PDSI			
Filter 1	-1	17%	10%	16%
	-2	16%	12%	12%
	-3	11%	11%	11%
	-4	8%	8%	8%
Filter 2	-1	14%	8%	13%
	-2	13%	9%	9%
	-3	9%	8%	8%
	-4	7%	6%	7%

Table 3. Percent of original series remaining in filtered series.

listed in Table 4. The largest 50-year and 75-year average area of drought occured in the first half of the 1600's and 1700's, the smallest average area of drought occured in the last half of the 1600's and very early 1700's, the period of the Maunder Minimum.

As part of our study of the spatial distributions of drought, we have constructed year-by-year maps of reconstructed July PDSI back to A.D. 1601. The objective is to determine whether a preferred drought area can be defined. The results of this work, which is still in progress, possibly could be used to help identify preferred modes of atmospheric circulation associated with large-scale drought. If the implied drought area-solar variation connection can be statistically verified the task of demonstrating causal mechanisms will necessarily involve atmospheric behavior.

Average Period	Maximum Drought Area	Minimum Drought Area
	PDSI $\leq$ -1	
10 year	1931-1940	1909-1918
20 year	1845-1864	1603-1622
25 year	1841-1865	1601-1625
50 year	1623-1672	1666-1715
75 year	1791-1865	1660-1734
	PDSI $\leq$ -2	
10 year	1931-1940	1909-1918
20 year	1845-1864	1605-1624
25 year	1841-1865	1601-1625
50 year	1708-1757	1658-1707
75 year	1715-1789	1641-1715
	PDSI $\leq$ -3	
10 year	1839-1848	1944-1953
20 year	1716-1735	1913-1932
25 year	1841-1865	1601-1625
50 year	1708-1757	1658-1707
75 year	1715-1789	1633-1707

Table 4. Periods of maximum and minimum drought area from reconstructions based on Grid S-50. Values are shown for 10, 20, 25, 50 and 75 year average periods.

There is an apparent systematic change with time of the amplitudes of successive drought maxima in a manner resembling changes in the amplitude of the sunspot periodicity on the time scale of the Gleissberg cycle (88 years).

According to Brier (1961), spectrum analysis discards information regarding similar variations in amplitude modulation between time series and consequently the relationship cannot be studied by the coherency function (Fig.9). Our approach to the problem was to examine the bivariate correlation between amplitudes of drought maxima from the bandpass-filtered series, and the envelope of the Hale sunspot cycle at the time of the corresponding drought maxima (Fig.14).

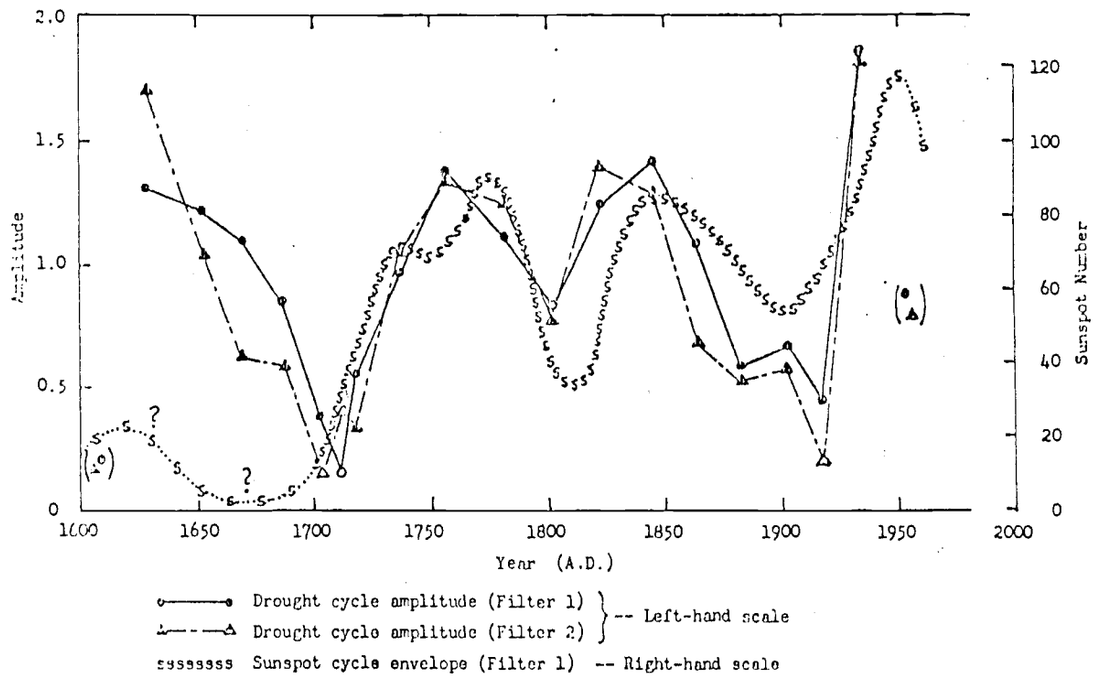

Filter 14. Chronology 1600-1962 A.D. of variations in amplitude of 22-year drought rhythm (averages of all DAI series) based on each of two band-pass filters, and chronology of Hale sunspot envelope. Sunspot data for period 1600-1700 are tentative reconstructions from J. Eddy.

A time series of appropriate values from the envelope of the sunspot series were correlated with corresponding time series of drought maxima from each filtered drought series. The individual correlation coefficients for the various series are given in Table 5.

In addition, a "weighted mean" correlation coefficient was computed between the sunspot envelope and a time series of drought maximum derived by the following steps:

1) The maxima series for each of the 3 reconstructed series of PDSI $\leq$ -1 was rescaled to have an average value of 1. The resulting rescaled series were averaged together yielding a "mean" series for PDSI $\leq$ -1 that incorporated information from reconstructions based on all 3 tree-ring grids.

2) Step 1 was repeated for PDSI $\leq$ -2, -3, and -4 series, resulting in a 4 "mean" series.

3) A weighted average of the 4 series resulting from step 2 was computed; the largest weight was on PDSI $\leq$ -1 and the smallest on PDSI $\leq$ -4, based on the rationale that the reconstructions considered to contain the least "noise" should be weighted most heavily.

The resulting correlation coefficient was 0.71 for the drought series filtered by filter No.1, and 0.59 for the series filtered by filter No.2, with significance limits of 1% and 5%, respectively.

TABLE 5

CORRELATION BETWEEN DROUGHT CYCLE AMPLITUDE AND ENVELOPE OF HALE SUNSPOT CYCLE*

1700 - 1962 A.D.

PDSI LIMIT	DAI FAMILY	FILTER 1			FILTER 2		
		NUMBER MAXIMA	CORRELATION COEFFICIENT	SIG. # LEVEL	NUMBER MAXIMA	CORRELATION COEFFICIENT	SIG. # LEVEL
-1	S-40	12	.645	.05	11	.548	--
	S-50	12	.683	.02	11	.685	.02
	F-65	12	.365	--	11	.209	--
-2	S-40	12	.555	--	11	.557	--
	S-50	12	.571	--	11	.554	--
	F-65	12	.550	--	12	.386	--
-3	S-40	12	.522	--	11	.554	--
	S-50	12	.544	--	11	.634	.05
	F-65	12	.555	--	11	.456	--
-4	S-40	11	.511	--	10	.506	--
	S-50	11	.770	.01	11	.776	.005
	F-65	12	.338	--	11	.371	--

*Envelope of Hale sunspot numbers filtered by Filter 1
#Two-tailed test (significance .05 or higher)

Conclusion

The results of our research offer significant statistical evidence that large-scale drought in western North America (as measured by area) has a rhythmic recurrence near 22 years that is significiently correlated to the 22 year Hale solar magnetic cycle. However, the percentage of the total variation in drought area accounted for by this periodic component is not large, roughly in the 10 to 15 percent range. Although our results do not allow us to specify that drought occurs in a near 22 year periodicity at any given location they do allow us to warn that the probability of drought occurrence will increase every 22 years.

From the viewpoint of solar physics and solar terrestrial mechanisms of potential relevance to climate, the results strongly suggest a connection between solar magnetic signals and wide-spread drought in western North America. This connection may be either direct or indirect. Our present thinking is that solar magnetic variation is not to be construed as a prime mover of large-scale drought, or of climatic aberrations resulting in drought. Also, it is our impression that the solar magnetic forcing function (if indeed it is one) acts more in the nature of a modulating mechanism, alternately favoring or suppressing large-scale development of drought when terrestrial climatic factors unrelated to solar variation are tending to encourage drought occurrence. Obviously the solar variation signal we may see in the drought area series is of such a small magnitude that the signal to noise ratio is quite small. It then follows that the drought-solar variation relationship we have described should not now be construed as a reliable basis for operational drought prediction.

ACKNOWLEDGEMENTS

Part of this research has been supported by the Atmospheric Sciences Section, National Science Foundation under grant DES 74-24163 and by the Climate Dynamics Program, Cliamte Dynamics Research Section, Division of Atmospheric Sciences, National Science Foundation under grant ATM 76-08493 and ATM 77-26189. A portion of the work was completed while J. M. Mitchell was affiliated with NCAR Advanced Study Program. H. C. Fritts and staff at the Laboratory of Tree-Ring Research provided assistance in computation of the F-65 reconstructions.

LITERATURE CITED

Bitvinskas, T. T., 1974. "Dendroclimatic Investigations." Gidrometeoizdat, Leningrad.

Blasing, T. J., 1978. Time series and multivariate analysis in paleoclimatology. From Time Series and Ecological Processes. H. H. Shugart, Jr., editor. SIAM-SIMS Conference Series No.5. Society for Industrial and Applied Mathematics, Philadelphia, PA.

Box, G. E. P., and G. M. Jenkins, 1976. Time Series Analysis: Forecasting and Control (revised edition). Holden-Day, Inc., San Francisco, California.

Douglass, A. E., 1919. Climatic cycles and tree growth. Carnegie Institution of Washington, Pub. No. 289, Vol. I.

_____, 1928. Climatic cycles and tree growth. Carnegie Institution of Washington, Pub. No. 289, Vol. II.

_____, 1936. Climatic cycles and tree growth. Carnegie Institution of Washington, Pub. No. 289, Vol. III.

_____, 1946. Researches in dendrochronology. University of Utah Bulletin, Vol. 37, No. 2. Biological Series Vol. 10, No. 1.

Eddy, John A., 1976. The Maunder Minimum. Science, Vol. 192, 1189-1202

Fritts, H. C., T. J. Blasing, B. P. Hayden, and J. E. Kutzbach, 1971. Multivariate techniques for specifying tree growth and climatic relationships and for reconstructing anomalies in paleoclimate. Journal of Applied Meteorology, Vol. 10, No. 5, 845-964.

Fritts, H. C., and D. J. Shatz, 1975. Selecting and characterizing tree-ring chronologies for dendroclimatic analysis. Tree-Ring Bulletin 35, 31-40.

Fritts, H. C., 1976. Tree Rings and Climate. Academic Press, London.

Glahn, H. R., 1968. Canonical correlation and its relationship to discriminant analysis and multiple regression. Journal of the Atmospheric Sciences, Vol. 25, 23-31.

Jenkins, G. M. and D. G. Watts, 1968. Spectral Analysis and Its Applications. Holden-Day, San Francisco, California.

Kutzbach, John E., 1967. Empirical eigenvectors of sea-level pressure, surface temperature and precipitation complexes over North America. Journal of Applied Meteorology, Vol. 6, No. 5, 791-802.

LaMarche, Valmore C., Jr. and H. C. Fritts, 1972. Tree-rings and sunspot numbers. Tree-Ring Bulletin, Vol. 32, 21-35.

Lawson, Merlin P. and C. W. Stockton, 1977. Exploration of the Great American Desert in the context of climatic reality: presented at the 73rd annual meeting of the Association of American Geographers, Salt Lake City, Utah, April 24-27, 1977.

Mitchell, J. M., Jr., C. W. Stockton, and D. M. Meko, 1978. An apparent 20+ year periodicity in drought occurrence in western United States (tenative): to be submitted to Science (in preparation).

_____, 1979. Evidence of a 22-year rhythm of drought in the western United States related to the Hale Solar Cycle since the 17th Century. In Proceddings: Solar-Climate Conference held at Ohio State University, August 24-28, (in print).

Palmer, W. C., 1964. Climatic variability and crop production. Proceedings of a seminar on "Weather and Our Food Supply," Center for Agricultural and Economic Development, CAED Report 20, Iowa State University, Ames, Iowa, 173-187.

_____, 1965. Meteorological drought. U. S. Weather Bureau Research Paper 45, U. S. Dept. of Commerce, Washington, D. C. 58p.

Roberts, Walter Orr, 1973. Relationships between solar activity and climatic change. Unpublished manuscript.

Sirén, G., and P. Hari, 1971. Coinciding periodicity in recent tree rings and glacial clay sediments. Rep. KEVO Subarctic Res. Sta. 8, 155-157.

Stockton, C. W., 1975. Long-term streamflow records reconstructed from tree-rings. Papers of the Laboratory of Tree-Ring Research, No. 5, The University of Arizona Press, Tucson.

Stokes, M. A. and T. L. Smiley, 1968. An Introduction to Tree-Ring Dating. The University of Chicago Press, Chicago.

Thompson, L. M., 1973. Cyclical weather patterns in the middle latitudes. Journal of Soil and Water Conservation, Vol. 28, 87-89.

Thornthwaite, C. W., 1948. "An approach toward a rational classification of climate." Geographical Review, Vol. 38, pp. 55-94.

Thornthwaite, C. W., and J. R. Mather, 1955. "The water balance." Drexel Inst. Tech. Publ. Climatol. Vol 8 (1), 1-104, Centerton, New Jersey.

Trewartha, Glenn T., 1961. The Earth's Problem Climates. The University of Wisconsin Press, Ltd., Madison. 334p.

Webb, Thompson III and D. R. Clark, 1977. Calibrating micropaleontological data in climatic terms: A critical review. Annals of the New York Academy of Sciences, Vol. 288, 93-118.

Willett, H. C., 1965. Solar-climatic relationships in the light of standardized climatic data. Journal of Atmospheric Sciences, Vol. 22, 120.

APPENDIX I

DERIVATION OF TRANSFER FUNCTIONS

A brief mathematical summary of the technique used to derive the transfer functions follows. Additional details can be found in papers by Glahn (1968), Webb and Clark (1977) and Blasing (1978). The following description mainly follows that of Blasing (1978).

General Procedure for Deriving Transfer Functions

1) Calculate eigenvectors of tree-ring data and PDSI, so that original data is expressed in terms of a reduced set of time series of eigenvector-amplitudes.

2) Select eigenvectors to be retained for subsequent canonical correlation and regression.

3) Determine regression equations for estimate of amplitudes of PDSI eigenvectors from observed amplitudes of tree-ring eigenvectors.

4) Reconstruct the long-term series of amplitudes of PDSI eigenvectors.

5) Transform the reconstructed eigenvector-amplitudes of PDSI into reconstructed PDSI at each of the original grid points or regions.

Symbols:

p number of tree-ring sites

q number of PDSI regions

n_1 number of years of tree-ring data used in eigenvector analysis

n_2 total number of years of PDSI used in eigenvector analysis

n_3 number of years in calibration period

r_1 number of eigenvectors of tree-ring indices retained for canonical analysis

r_2 number of eigenvectors of PDSI retained for canonical analysis

${}_nX_p$ tree-ring indices for n years at p sites

${}_nX^*_p$ standarized tree-ring series -- series for each site has mean of zero and standard deviation of 1

${}_pE_i$ eigenvectors of tree-ring indices; i eigenvectors ($i \leq p$) each consisting of weights on p tree-ring sites

${}_pR_p$ correlation matrix of tree-ring data

${}_pL_p$ diagonal array of eigenvalues from tree-ring data

${}_nC_i$ amplitudes (also called principal components or scores) of i tree-ring eigenvectors for n years

${}_nC^*_i$ standardized amplitudes of tree-ring eigenvectors -- amplitudes for each of i eigenvectors has mean of 0) and standard deviation of 1

${}_nY_q$ Palmer index (PDSI) for n years in q regions

$_{n}Y^{*}_{q}$ standarized PDSI

$_{n}\bar{Y}_{q}$ means of PDSI in each q regions -- each column has n identical values equal to the mean for a particular region

$_{q}S_{y_q}$ diagonal matrix of standard deviations of PDSI in q regions

$_{q}F_{i}$ eigenvectors of PDSI i eigenvectors ($i \leq q$), each consisting of weights on q regions

$_{q}P_{q}$ correlation matrix of PDSI

$_{q}M_{q}$ diagonal array of eigenvectors from PDSI

$_{n}D_{i}$ amplitudes of i PDSI eigenvectors ($i \leq q$) for n years

$_{n}D^{*}_{i}$ standardized amplitudes of PDSI eigenvectors

$_{n}\bar{D}_{i}$ means of amplitudes of each of i PDSI eigenvectors, calculated over n years

$_{i}S_{D_i}$ diagonal array of standard deviations of amplitudes of i eigenvectors of PDSI

$_{i}S^{*}_{D_i}$ diagonal array of standard deviations of standarized PDSI amplitudes (equals the identity matrix, since these amplitudes have standard deviations of i by definition)

$_{n_3}C^{*}_{r_1}H_{r_2}$ linear combinations of amplitudes of tree-ring eigenvectors in canonical correlation

$_{n_3}D^{*}_{r_2}G_{r_2}$ linear combinations of amplitudes of PDSI eigenvectors

$_{r_1}H_{r_2}, _{r_2}G_{r_2}$ transformation matrices calculated during canonical correlation

$_{r}I_{r}$ identity matrix

$_{r}\Lambda_{r}$ diagonal matrix of canonical correlations

$_{r_1}B_{r_2}$ matrix of regression equations from canonical analysis

Step 1. CALCULATE EIGENVECTORS

(A) Tree-ring indices

Each column of $_{p}E_{p}$ is an eigenvector extracted from the correlation matrix of the original tree-ring data, and is defined such that:

1. $$_{p}R_{p} \; _{p}E_{p} = {}_{p}E_{p} \; L_{p}$$

where $_{p}R_{p} = 1/n \; (\; _{p}X^{*}{}'_{n_1} \; X^{*}_{p} \;)$ is the correlation matrix based on the full n years of tree-ring data, $_{p}L_{p}$ is a diagonal array of eigenvalues, and $_{n_1}X_{p}$ is a matrix of standarized tree-ring indices.

The amplitudes of the eigenvectors are:

2. $$_{n_1}C_{p} = {}_{n_1}X^{*}{}_{p} \; E_{p}$$

Equation 2 expresses the original tree-ring time series in terms of n observations of the amplitudes of p eigenvectors. The eigenvectors are orthogonal; each one represents an independent part of the original variance.

The original data can be approximated by an subset of r_1 eigenvectors ($r_1 \leq p$) with amplitudes:

3. $$_{n_1}C_{r_1} = {}_{n_1}X^{*}{}_{p} \; E_{r_1}$$

These amplitudes can also be expressed in standarized form -- mean of 0,

standard deviation of 1. Standardized forms of the amplitudes will be denoted by $_{n_1}C^*_p$ or $_{n_1}C^*_{r_1}$ in this appendix.

(B) PDSI

Eigenvectors, $_qF_q$, of PDSI are calculated from the correlation matrix, $_qP_q$, of PDSI such that:

4. $$_qP_q \quad F_q = {}_qF_q \quad M_q$$

where $_qP_q = 1/n_2 \; (\; _qY'^*_{n_2} \; Y^*_q \;)$ in the correlation matrix of PDSI based on the full n_2 years of PDSI data, $_qM_q$ is a diagonal array eigenvalues, and $_{n_2}Y^*_q$ is the matrix of standardized PDSI data.

By analogy with equations 2 and 3, amplitudes of PDSI eigenvectors are:

5. $$_{n_2}D_q = {}_{n_2}Y^*_q \quad F_q$$

and

6. $$_{n_2}D_{n_2} = {}_{n_2}Y^*_q \quad F_{r_2}$$

where $r_2 \leq q$

The corresponding standardized amplitudes are denoted by $_{n_2}D^*_q$ and $_{n_2}D^*_{r_2}$.

Step 2. SELECT EIGENVECTORS FOR FURTHER ANALYSIS

Step 1 yielded time series of amplitudes, $_{n_1}C_p$ and $_{n_2}D_q$, of 'p' eigenvectors of tree-ring indices and 'q' eigenvectors of PDSI. These data were expressed by $_{n_1}C^*_p$ and $_{n_2}D^*_q$ in standardized form. The overlap between the n_1 years of tree-ring data and n_2 years of PDSI

is the n_3 years defined here as the calibration period.

Before proceeding to canonical correlation and regression some eigenvectors are usually dropped from the analysis. Varying degrees of subjective reasoning may go into the decision. For example, many of the lower eigenvectors of tree-ring indices may contribute little to the total variance, and may indeed reflect merely noise; or the spatial patterns given by some PDSI eigenvectors may not seem reasonable from a climatological point of view. For the rest of this development, it is assumed that, by some method, reduced sets of r_1 tree-ring eigenvectors and r_2 PDSI eigenvectors have been selected for further analysis.

In this particular study for comparison with Grids S-40 and F-65 we chose the first 5 PDSI eigenvectors because of the high percentage of the original PDSI variance they explained (in the case of Grid S-50, 7 PDSI eigenvectors were retained). We then calculated the correlation matrix between amplitudes of PDSI eigenvectors at year t and tree-ring eigenvectors at years t and $t + 1$. Tree-ring eigenvector-amplitudes highly correlated with PDSI amplitudes were selected as predictors. Six tree-ring eigenvectors -- 3 at year t, 3 at year t+1 -- were chosen; thus in the case of Grid S-40, $r_1 = 6$ and $r_2 = 5$.

Step 3. DETERMINE REGRESSION EQUATIONS

Step 2 yielded time series of amplitudes, ${}_{n_3}C^*_{r_1}$ and ${}_{n_3}D^*_{r_2}$, of tree-ring eigenvectors and PDSI eigenvectors, where

n_3 = number of years in calibration period,

r_1 = number of tree-ring eigenvectors retained, and

r_2 = number of PDSI eigenvectors retained.

Next, canonical correlation and regression (Glahn 1968, Blasing 1978) are used to derive regression coefficients that can be used to predict amplitudes of PDSI eigenvectors from observations of amplitudes of tree-ring eigenvectors.

Canonical correlation yields linear combinations, ${}_{n_3}C^*_{r_1}\,H_{r_2}$ and ${}_{n_3}D^*_{r_2}\,G_{r_2}$, such that:

7. $${}_{r_2}H'_{r_1}\,C^{*\prime}_{n_3}\,C^*_{r_1}\,H_{r_2} = (n_3)_{r_2}\,I_{r_2},$$

8. $${}_{r_2}G'_{r_2}\,D^{*\prime}_{n_3}\,D^*_{r_2}\,G_{r_2} = (n_3)_{r_2}\,I_{r_2}, \text{ and}$$

9. $${}_{r_2}H'_{r_1}\,C^{*\prime}_{n_3}\,D^*_{r_2}\,G_{r_2} = (n_3)_{r_2}\,\Lambda_{r_2}$$

Where ${}_{r_1}H_{r_2}$ and ${}_{r_2}G_{r_2}$ are transformation matrices,

${}_{r_2}I_{r_2}$ is the identity matrix, and

${}_{r_2}\Lambda_{r_2}$ is a diagonal matrix of canonical correlation coefficients.

The linear combination ${}_{n_3}D^*_{r_2}\,G_{r_2}$ can be predicted in a least-squares sense from the linear combination ${}_{n_3}C^*_{r_1}\,H_{r_2}$ by:

10. $${}_{n_3}\widehat{D^*_{r_2}\,G_{r_2}} = {}_{n_3}C^*_{r_1}\,H_{r_2}\,\Lambda_{r_2}$$

Where the $\widehat{\ }$ denotes a predicted quantity.

The "first" pair of functions, defined by the first columns of ${}_{r_1}H_{r_2}$ and ${}_{r_2}G_{r_2}$ are as highly correlated as any other possible pair of functions, and the correlation coefficient equals the uppermost element of the diagonal matrix ${}_{r_2}\Lambda_{r_2}$. The pair of functions in the second columns have the next highest correlation; and each is uncorrelated with either of the first pair of functions, and so forth.

Equation 10 can be rearranged to yield predictions of amplitudes, $\hat{D}^*$, of PDSI eigenvectors. The form of the equation depends on how many canonical correlations are retained:

If all elements of ${}_{r_2}\Lambda_{r_2}$ are retained:

11. $${}_{n_3}\hat{D}^*_{r_2} = {}_{n_3}C^*_{r_1}\,{}_{r_2}H_{r_2}\,{}_{r_2}\Lambda_{r_2}\,{}_{r_2}G^{-1}_{r_2}$$

If some elements of ${}_{r_2}\Lambda_{r_2}$ are considered insignificant, they may be set equal to zero, and :

12. $${}_{n_3}\hat{D}^*_{r_2} = {}_{n_3}C^*_{r_1}\,{}_{r_2}H_{r_2}\,{}_{r_2}\Lambda_{r_2}\,{}_{r_2}G'_{r_2}\,{}_{r_2}S_D{}^*_{r_2},$$

Where some elements of ${}_{r_2}\Lambda_{r_2}$ are equal to zero, and ${}_{r_2}S_D{}^*_{r_2}$ is the variance matrix of ${}_{n_3}D^*_{r_2}$.

Equations 11 and 12 are now in the form of regression equations, with a matrix of regression coefficients ${}_{r_1}B_{r_2}$ such that:

13. $${}_{n_3}\hat{D}^*_{r_2} = {}_{n_3}C^*_{r_1}\,{}_{r_1}B_{r_2},$$

Where ${}_{r_1}B_{r_2} = {}_{r_1}H_{r_2}\,{}_{r_2}\Lambda_{r_2}\,{}_{r_2}G^{-1}_{r_2}$ for equation 11 and

${}_{r_1}B_{r_2} = {}_{r_1}H_{r_2}\,{}_{r_2}\Lambda_{r_2}\,{}_{r_2}G'_{r_2}\,{}_{r_2}S_D{}^*_{r_2}$ in equation 12.

Step 4. RECONSTRUCT AMPLITUDES OF PDSI EIGENVECTORS

Equation 13 predicts amplitudes (standardized) of eigenvectors of PDSI from observed amplitudes (standardized) of tree-ring eigenvectors. The long-term series of PDSI amplitudes can be reconstructed by substituting the long-term series, ${}_{n_1}C^*_{r_1}$, of tree-ring amplitudes on the right side of

equation 13:

14. $$\hat{{}_{n_1}D^{*}_{r_2}} = {}_{n_1}C^{*}_{r_1}\,{}_{r_1}B_{r_2}$$

Step 5. TRANSFORM FROM EIGENVECTOR-AMPLITUDES TO ORIGINAL PDSI

The standardized amplitudes $\hat{{}_{n_1}D^{*}_{r_2}}$ can be rewritten in terms of the unstandardized amplitudes as:

15. $$\hat{{}_{n_1}D^{*}_{r_2}} = [\,\hat{{}_{n_1}D_{r_2}} - {}_{n_1}\bar{D}_{r_2}\,]\;{}_{r_2}S^{-1}_{D_{r_2}}$$

where ${}_{n_1}\bar{D}_{r_2}$ contains the column means of ${}_{n_1}D_{r_2}$ and ${}_{r_2}S_{D_{r_2}}$ the column standard deviations.

Similarly, the standardized PDSI $\hat{{}_{n_1}Y^{*}_{q}}$ can be rewritten in terms of unstandardized PDSI as:

16. $$\hat{{}_{n_1}Y^{*}_{q}} = [\,\hat{{}_{n_1}Y_{q}} - {}_{n_1}\bar{Y}_{q}\,]\;{}_{r_2}S_Y{}^{-1}{}_{r_2}$$

Substitute [15] into [14] to get:

17. $$[\,\hat{{}_{n_1}D_{r_2}} - {}_{n_1}\bar{D}_{r_2}\,]\;{}_{r_2}S^{-1}{}_{D_{r_2}} = {}_{n_1}C^{*}_{r_1}\,{}_{r_1}B_{r_2}$$

Rearrange [17] to get:

18. $$\hat{{}_{n_1}D_{r_2}} = {}_{n_1}C^{*}_{r_1}\,{}_{r_1}B_{r_2}\,{}_{r_2}S_{D_{r_2}} + {}_{n_1}\bar{D}_{r_2}$$

Equation 18 gives predictions of amplitudes of r_2 PDSI eigenvectors. The next step is to express the prediction in terms of PDSI at the original q grid points (regions).

Substitute [6] into [18] and rearrange to get:

19. $$\hat{{}_{n_2}Y^{*}_{q}}\ F_{r_2} = {}_{n_1}C^{*}_{r_1}\ B_{r_2}\ S_{D_{r_2}} + {}_{n_1}\bar{D}_{r_2} \quad \text{and}$$

20. $$\hat{{}_{n_2}Y^{*}_{q}} = \{\ {}_{n_1}C^{*}_{r_1}\ B_{r_2}\ S_{D_{r_2}} + {}_{n_1}\bar{D}_{r_2}\ \}\ {}_{r_2}F'_{q}$$

Equation [20] gives reconstructions of standardized PDSI.

For unstandarized PDSI, substitute [16] into [20] and rearrange:

21. $$\hat{{}_{n_1}Y_{q}} = \{\ {}_{n_1}C^{*}_{r_1}\ B_{r_2}\ S_{D_{r_2}} + {}_{r_1}\bar{D}_{r_2}\ \}\ {}_{r_2}F'_{q}\ S_{r_q} + {}_{n_1}\bar{Y}_{q}$$

Equation 21 yields the desired reconstructions of PDSI at the original q grid points. Of the quantities on the right ${}_{q}S_{Y_q}$ and ${}_{n_1}\bar{Y}_{q}$ are standard deviations and means of PDSI from the calibration period, ${}_{r_2}S_{D_{r_2}}$ and ${}_{n_1}\bar{D}_{r_2}$ are calculated from reconstructed PDSI eigenvector amplitudes, ${}_{r_1}B_{r_2}$ is output from the canonical regression analysis, ${}_{r_2}F'_{q}$ is output from eigenvector analysis of PDSI, and ${}_{n_1}C^{*}_{r_1}$ is output from eigenvector analysis of the tree-ring indices.

Variations of the General Procedure Applied to this Study

1) PDSI eigenvectors are computed from the COVARIANCE matrix instead of the correlation matrix. The factor $_{r_2}S^{-1}{}_{Y}{}_{r_2}$ thus would not appear in [16] or [21]. The rest of the analysis is unchanged.

2) Lagged amplitudes of tree-ring eigenvectors were used as 3 of the 6 predictors in Grids S-40 and F-65 and 4 of the 6 predictors in Grid S-50 in the canonical regression of Step 3. The matrix $_{n_3}C^{*}{}_{r_1}$ as it appears in [7] and afterwards is thus not merely a subset of the original $_{n_3}C^{*}{}_{p}$ amplitudes. For example, for Grid S-40, the row corresponding to year 1800 contains amplitudes of 3 eigenvectors corresponding to 1800 and of 3 others corresponding to 1801.

3) For Grid S-40:

p = 40 tree-ring sites q = 40 regions

n_1 = 264 years n_2 = 40 years n_3 = 32 years

r_1 = 6 eigenvectors r_2 = 5 eigenvectors

For Grid S-50:

p = 50 tree-ring sites q = 40 regions

n_1 = 364 years n_2 = 40 years n_3 = 32 years

r_1 = 2 eigenvectors r_2 = 7 eigenvectors

(6 variables included in constant after lagging)

For Grid F-65:

p = 65 tree-ring sites q = 40 regions

n_1 = 364 years n_2 = 40 years n_3 = 32 years

r_1 = 3 eigenvectors r_2 = 5 eigenvectors

(6 variables included in canonical after lagging)

4) In all 3 cases, all canonical correlations were retained in the regression; therefore, equations [11] applied rather than [12].